Determination of the Rate Coefficients of the $SO_2 + O + M \rightarrow SO_3 + M$ Reaction

S. M. HWANG,[1] J. A. COOKE,[1] K. J. DE WITT,[1,†] M. J. RABINOWITZ[2]

[1]*Department of Chemical Engineering, University of Toledo, Toledo*, OH 43606
[2]*Research and Technology Directorate*, NASA *Glenn Research Center at Lewis Field, Mail Stop* 5-10, *Brook Park*, OH 44135

Received 22 April 2009; revised 17 July 2009, 2 October 2009; accepted 5 October 2009

DOI 10.1002/kin.20472
Published online in Wiley InterScience (www.interscience.wiley.com).

ABSTRACT: Rate coefficients of the title reaction R_{31} ($SO_2 + O + M \rightarrow SO_3 + M$) and R_{56} ($SO_2 + HO_2 \rightarrow SO_3 + OH$), important in the conversion of S(IV) to S(VI), were obtained at T = 970–1150 K and $\rho_{ave} = 16.2$ μmol cm^{-3} behind reflected shock waves by a perturbation method. Shock-heated H_2/O_2/Ar mixtures were perturbed by adding small amounts of SO_2 (1%, 2%, and 3%) and the OH temporal profiles were then measured using laser absorption spectroscopy. Reaction rate coefficients were elucidated by matching the characteristic reaction times acquired from the individual experimental absorption profiles via simultaneous optimization of k_{31} and k_{56} values in the reaction modeling (for satisfactory matches to the observed characteristic times, it was necessary to take into account R_{56}). In the experimental conditions of this study, R_{31} is in the low-pressure limit. The rate coefficient expressions fitted using the combined data of this study and the previous experimental results are $k_{31,0}/[Ar] = 2.9 \times 10^{35}\ T^{-6.0} \exp(-4780\ K/T) + 6.1 \times 10^{24}\ T^{-3.0} \exp(-1980\ K/T)$ $cm^6\ mol^{-2}\ s^{-1}$ at T = 300–2500 K; $k_{56} = 1.36 \times 10^{11} \exp(-3420\ K/T)$ $cm^3\ mol^{-1}\ s^{-1}$ at T = 970–1150 K. Computer simulations of typical aircraft engine environments, using the reaction mechanism with the above $k_{31,0}$ and k_{56} expressions, gave the maximum S(IV) to S(VI) conversion yield of ca. 3.5% and 2.5% for the constant density and constant pressure flow condition, respectively. Moreover, maximum conversions occur at

Correspondence to: Martin J. Rabinowitz; e-mail: martin.j.rabinowitz@nasa.gov.

Present address of S. M. Hwang: Department of Mechanical, Industrial, and Manufacturing Engineering, University of Toledo, Toledo, OH 43606.

Present address of J. A. Cooke: GE Oil & Gas, 1480 Valley Parkway, Bethlehem, PA 18017.

Contract grant sponsor: NASA Glenn Research Center.

Contract grant number: NRA-01-GRC02 Phase 2, no. IC-02-25.

Supporting Information related to thermodynamic data (Table 1), reaction mechanism (Table 2), and experimental conditions and results (Table 3) is available in the online issue at www.interscience.wiley.com.

[†]Deceased.

rather higher temperatures (~1200 K) than that where the maximum $k_{31,0}$ value is located (~800 K). This is because the conversion yield is dependent upon not only the $k_{31,0}$ and k_{56} values (production flux) but also the availability of H, O, and HO_2 in the system (consumption flux). © 2010 Wiley Periodicals, Inc.* Int J Chem Kinet 42: 168–180, 2010

INTRODUCTION

Contrails and contrail-induced cirrus clouds may affect the global climate via radiative forcing and the alteration of atmospheric chemistry [1–3]. The critical chemical species in contrails, in addition to soot, ions, and water vapor, are sulfates and sulfuric acid formed by oxidation of fuel sulfur, i.e., low oxidation state fuel bound S(II), mostly thiols and sulfides, are rapidly and nearly quantitatively converted to S(IV), i.e., SO_2, in the high-temperature oxidative environment of the combustor, and then on to S(VI), mostly SO_3 and small amounts of sulfates, formed in the cooler, but still harsh environment of the turbine and exhaust nozzle [4–6]. Sulfates and sulfuric acid, formed in the aircraft exhaust plume, enhance the formation of contrails and cirrus clouds through homogeneous binary nucleation of H_2SO_4/H_2O and heterogeneous condensation of H_2SO_4/H_2O on soot particles or ions [4–9].

Owing to the significant role of S(VI) (SO_3 and H_2SO_4) in the formation of contrail and cirrus cloud, the conversion fraction of S(IV) to S(VI) has been measured or calculated by various authors: The measured fractions were about 0.34%–4.5% [10,11] or 3.3% ± 1.8% [12], while calculations from measured particulate volume, presuming only H_2SO_4 and H_2O are in the particles, span a wide range from 0.4% to 80% [10,11,13–15].

The route to sulfuric acid formation in the homogeneous gas phase has been considered as R_0 (fuel-bound $S \rightarrow\rightarrow SO_2$), R_{31} ($SO_2 + O + M \rightarrow SO_3 + M$), R_{32} ($SO_2 + OH\ (+M) \rightarrow HOSO_2\ (+M)$), R_{52} ($HOSO_2 + O_2 \rightarrow SO_3 + HO_2$), and R_{57} ($SO_3 + H_2O \rightarrow H_2SO_4$). It is believed that R_0 occurs inside the combustor, R_{31}, R_{32}, and R_{52} in the turbine and engine exit nozzle, and R_{57} in the exhaust plume. R_{31} is considered as the principal reaction pathway for the conversion of sulfur from the S(IV) to the S(VI) oxidation state. As seen in Fig. 6, the experimentally measured rate coefficients of the spin-forbidden R_{31} ($SO_2(X^1A_1) + O(^3P) + M \rightarrow SO_3(X^1A_1') + M$) exhibit an unusual behavior—an increase with temperature ($T <$ ~450 K) [16,17] followed by a sharp decrease with further increase of temperature ($T >$ ~1400 K) [18–20]. This unusual behavior of rate coefficients with respect to temperature was first rationalized by Astholz et al. [19] in terms of potential energy barrier arising from the triplet–singlet intersystem crossing and diminishing collision efficiency with temperature in the stabilization of the collision complex formed (see the section Discussion for details).

Despite its important role in contrail formation, the rates of this reaction have never been measured at temperatures typical of aircraft operation (900–1200 K). Moreover, there are large discrepancies among the extrapolated values from the existing rate coefficient expressions to this temperature region. For example, at $T = 1000$ K the calculated or extrapolated values from the early studies are (in $cm^6\ mol^{-2}\ s^{-1}$) 2.8×10^{15} [21], 4.1×10^{15} [17], 9.6×10^{15} [16], 1.0×10^{16} [20], and 3.2×10^{16} [19]. An order of magnitude discrepancy is easily recognized. Recently, Naidoo et al. [22] measured the rate coefficients of R_{31} in the temperature range of 290–840 K and reported the Rice–Ramsperger–Kassel–Marcus (RRKM) fitted parameters for $k_{31,0}$/[Ar], $k_{31,\infty}$ and broadening factor F_c for $T = 220$–2500 K. The $k_{31,0}$/[Ar] value of Naidoo et al. at $T = 1000$ K gives 2.8×10^{15} $cm^6\ mol^{-2}\ s^{-1}$. We have previously reported results for this reaction over a more limited temperature range [23]. In the present work, we extended our previous efforts and completed the measurement of the rate coefficients of R_{31} at $T =$ 970–1150 K using a shock tube and OH laser absorption technique.

SELECTION OF EXPERIMENTAL CONDITIONS AND COMPUTER SIMULATION

Determination of the rate coefficients of R_{31} was performed via a perturbation method utilizing the abundant and well-characterized O-atoms provided by the shock-induced ignition of $H_2/O_2/Ar$ mixtures. This permitted the use of experimentally convenient mixture dilutions and reaction time scales as well as sensitive OH absorption diagnostics in the easily accessible near ultraviolet wavelength regime. We perturbed the $H_2/O_2/Ar$ reaction system with small amounts of SO_2 and recorded the differences in temporal behavior of the OH absorption. In this regard, construction of a robust reaction mechanism of the $SO_2/H_2/O_2/Ar$ system is essential. Our reaction mechanism is given in Table 2 in the Supporting Information.

For the temperature and pressure range relevant to S(IV) to S(VI) conversion, the major O-atom production reaction is R_1 ($H + O_2 \rightarrow OH + O$) and the

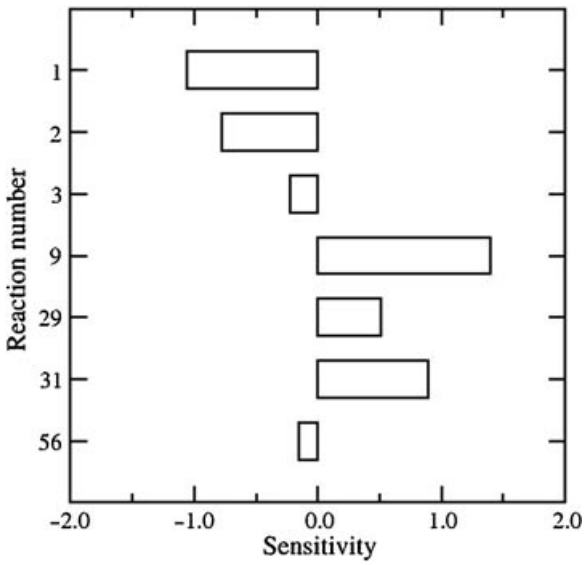

Figure 1 Sensitivity spectra for τ_{50} of the $SO_2/H_2/O_2/Ar =$ 2.0/0.5/10.0/87.5 mixture at $T = 1036$ K and $\rho = 15.8$ μmol cm^{-3} (Fig. 2 condition).

main O-atom consumption reaction is R_2 ($O + H_2 \rightarrow OH + H$). O-atom production rates are further modified by R_9 ($H + O_2 + M \rightarrow HO_2 + M$) through the channeling of some H-atoms away from chain branching. In the $SO_2/H_2/O_2/Ar$ system, R_{31} ($SO_2 + O + M \rightarrow SO_3 + M$) and R_2 compete for O-atoms. In rich $H_2/O_2/Ar$ mixtures, this competition would be dominated by R_2 and thus the addition of SO_2 would barely affect the course of reaction. Therefore, we restrict our consideration to lean $H_2/O_2/Ar$ mixtures only. On the basis of our previous study [24], we selected $H_2/O_2/Ar = 0.5/10.0/89.5$ ($\phi = 0.025$) as the baseline mixture. Using this mixture, we performed a series of sensitivity analyses to determine both the optimum levels of SO_2 addition and the best set of reaction characteristics to use. We determined that matching the characteristic times (τ_{max}, τ_{75}, τ_{50}, and τ_{25} defined in the Results section) and employing three mixtures containing 1.0%, 2.0%, and 3.0% SO_2 would give the best balance of overall reaction sensitivity and experimental convenience. Figure 1 shows sensitivity spectra obtained using the Table 2 reaction mechanism at a typical experimental condition. The sensitivity of R_{31} was found to be increased with both decreasing T and increasing SO_2/H_2 ratio in the mixture. Although excellent R_{31} sensitivities were computed at low temperatures, the characteristic times became prohibitively long.

The Table 2 mechanism was composed of 57 elementary reactions in 18 chemical species. For H_2/O_2 reactions, we used our reaction mechanism of 20 elementary reactions [24] with a change in k_{14} ($HO_2 + OH \rightarrow H_2O + O_2$) from 2.0×10^{13} to 3.0×10^{13} cm^3 mol^{-1} s^{-1} following the recommendation of Srinivasan et al. [25]. The H_2/O_2 reactions were combined with additional 35 reactions that are related to SO_2 oxidation by $H_xS_yO_z$ species from Rasmussen et al. [26]. Then we consider the oxidation of SO_2 by HO_2 radical, important in our experimental conditions, through the reaction R_{56} ($SO_2 + HO_2 \rightarrow SO_3 + OH$) of which rate coefficients are obtained as part of the simultaneous optimization with R_{31} (see below). Also, we added R_{57} ($SO_3 + H_2O \rightarrow H_2SO_4$) [27] for final product formation for completeness. However, the contribution of this reaction to the reaction progress is negligible.

All simulations were performed using our custom code that has advantageous built-in features for optimization. This code has been thoroughly tested against existing kinetic codes [28]. Recently updated values for the thermodynamic data [29,30] have been used for all species except for HOSO, HSO_2, and $HOSO_2$. The thermodynamic properties of these species were estimated using the available experimental data and theoretical calculations. The NASA polynomial coefficients of these species are given in Table 1 in the Supporting Information.

EXPERIMENTAL

The shock tube-laser absorption technique employed in this study is described in detail elsewhere [31]. Briefly, a rolled square stainless steel shock tube, 63.5 mm in cross section, was used for experiments. The test section was routinely pumped below 3 μTorr by a Varian V60 Turbopump. A combined leak and outgassing rate of the test section was 5 μTorr min^{-1}. To minimize problems due to wall loss of SO_2, all fills were done in a two-step process. First, the shock tube was filled with mixture to the desired starting pressure and the room temperature absorption of SO_2 was measured. The tube was then evacuated and refilled to the same pressure with fresh test gas. All shocks were then initiated within 1 min of admitting the test gas mixture.

Shock speeds were measured using four flush-mounted 113A21 PCB Piezotronics pressure transducers coupled to Phillips PM6666 programmable countertimers. The last pressure transducer was axially coincident with the center of the observation windows, 12.7 mm distant from the end wall. Measured shock speeds were fitted to a second-order polynomial in distance. The extrapolated speed to the end wall was used together with NASA thermodynamic data [29] in solving the relationships for the reflected shock properties [32], assuming full vibrational relaxation and no chemical reaction at the shock front. The postreflected shock

properties were corrected for boundary layer/reflected shock interaction effects using the methodology described by Hwang et al. [28].

The combined OH and SO_2 absorption profiles were measured at 310.032 nm (in air), corresponding to the $P_1(5)$ line of the (0,0) band of the OH $A^2\Sigma^+ \leftarrow X^2\Pi$ transition. UV light was produced by a CW argon ion laser (Coherent Innova 200) pumped ring-dye laser (Coherent 899-21) running Kiton Red 620 dye. Intracavity frequency doubling was achieved with an angle tuned $LiIO_3$ crystal. For absorption measurements, a triple beam scheme was employed: a probe beam passed through the center of two 25.4-mm-diameter S1-UVA quartz windows (12.7 mm distant from the shock tube end wall), an intensity reference beam, and a wavelength reference beam. Passage through an unconstrained burner-stabilized methane/air flame was used to provide the wavelength reference, i.e., the center absorption of the OH $P_1(5)$ line. Each detector was a combination of interference filter ($\lambda_0 = 310 \pm 10$ nm fwhm), a PMT (Thorn EMI9924QB), and a high-speed buffer/amplifier. A custom dynode chain was used for these experiments to assure the linearity of the absorption signal. The probe, reference, difference (probe dc–reference ac), and the last pressure transducer signals were recorded on a four-channel Nicolet 4094C digital oscilloscope equipped with Nicolet 4570 plug-in units. Reaction progress was followed using the difference signal. The S/N of the difference signal was usually better than 60. The overall electronic time constant determined for the entire PMT–buffer–cable system was less than 0.5 μs.

$SO_2/H_2/O_2/Ar$ test gas mixtures were prepared manometrically and allowed to stand for at least 48 h before use. A pump-fill-pump-fill cycle was used for the SO_2 addition to minimize the effect of wall loss. The maximum uncertainty in mixture composition was less than 0.5% of the nominal mole fraction for each component. The stated purities of the gases were H_2, 99.9995% (MG Industries, Malvern, PA; scientific grade); O_2, 99.998% (MG Industries; scientific grade); SO_2 (anhydrous), 99.98 wt% (MG Industries; scientific grade); Ar, 99.9999% (MG Industries; sputtering grade). All gases were used without further purification.

RESULTS

A typical absorption profile is shown in Fig. 2. The reflected shock passage at time zero is shown in the form of a schlieren peak at the extreme left-hand edge of the experimental trace. The initial absorption is entirely due to SO_2.

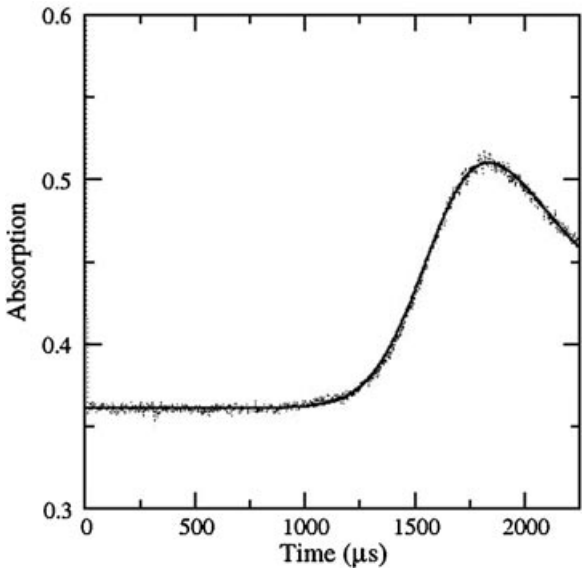

Figure 2 Typical experimental and simulated absorption profiles. $SO_2/H_2/O_2/Ar = 2.0/0.5/10.0/87.5$, $T = 1036$ K, and $\rho = 15.8$ μmol cm^{-3}.

Because both SO_2 and OH absorb 310-nm UV light, the absorption coefficients of SO_2 were measured and used in the simulation of experimental reaction progress. OH absorption coefficients were calculated using our recent values of the spectral line broadening parameters and other molecular properties [33]. The mean room temperature base e absorption coefficient of SO_2 measured by pump-fill-pump-fill method was $\varepsilon_e(SO_2) = (7.0 \pm 0.4) \times 10^4$ cm^2 mol^{-1}, which is about 30% smaller than the spectroscopic measurement of Vandaele et al. [34].

Figure 3 shows the SO_2 absorption coefficients measured at room temperature and at temperatures behind incident and reflected shock waves. A temperature-dependent fitting gives

$$\varepsilon_e(SO_2) = 1.3 \times 10^5 \exp(-180\ \mathrm{K}/T)\ \mathrm{cm}^2\ \mathrm{mol}^{-1}.$$

For reaction progress and sensitivity analyses, the following set of observables was obtained from an experimental absorption profile: an initial SO_2 absorption after reflected shock passage, $A_{SO_2,0} = 1 - I_{SO_2,0}/I_0$; a maximum absorption, $A_{max} = (1 - I/I_0)_{max}$; and four characteristic times (τ_{max}, τ_{75}, τ_{50}, and τ_{25}). Evaluation of τ_{max}, time to reach A_{max}, is straightforward. For τ_{25}, however, it was necessary to use a subtracted absorption signal ($A'_{max} = A_{max} - A_{SO_2,0}$) for the experiments that resulted in large $A_{SO_2,0}$ and small A_{max}. Thus τ_{25}, τ_{50}, and τ_{75} were defined as the time to reach 25%, 50%, and 75% of A'_{max}, respectively. Figure 4 shows τ_{50} values measured in 1.0%, 2.0%, and

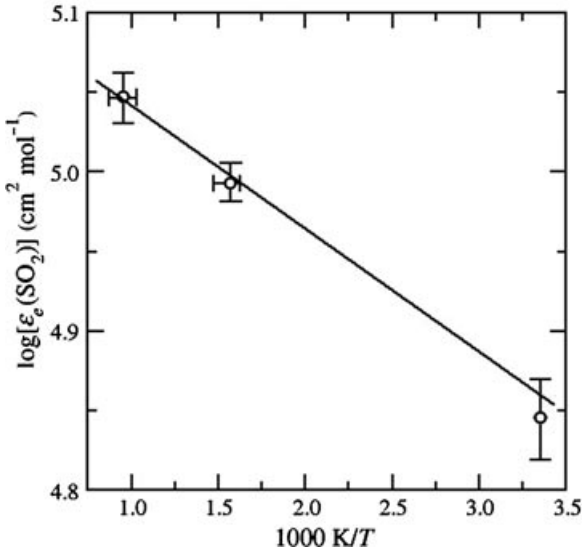

Figure 3 Base e absorption coefficients of SO_2 at 310 nm. The least-squares fit is $\varepsilon_e(SO_2) = 1.3 \times 10^5 \exp(-180\,K/T)$ cm^2 mol^{-1}. The vertical error bars represent error limits at the 95% confidence level.

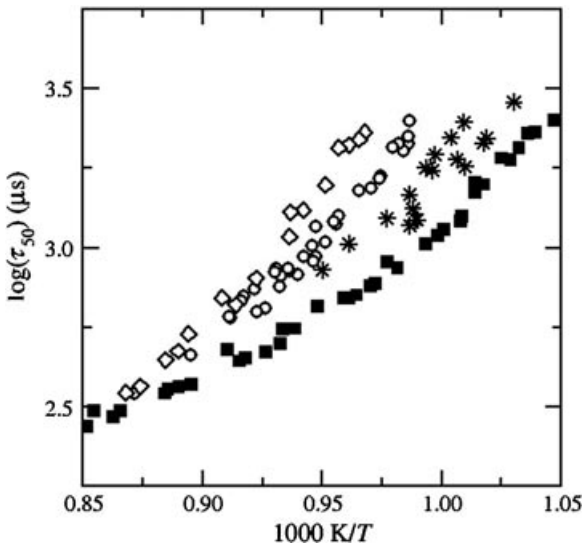

Figure 4 Measured τ_{50} values of the baseline and SO_2-perturbed mixtures. Symbols are as follows: filled square, $SO_2/H_2/O_2/Ar$ = 0.0/0.5/10.0/89.5 (base line mixture); star, $SO_2/H_2/O_2/Ar$ = 1.0/0.5/10.0/88.5; open circle, $SO_2/H_2/O_2/Ar$ = 2.0/0.5/10.0/87.5; open diamond, $SO_2/H_2/O_2/Ar$ = 3.0/0.5/10.0/86.5.

3.0% SO_2/0.5% H_2/10.0% O_2/Ar mixtures together with those from a baseline mixture (0.5% H_2/10.0% O_2/89.5% Ar). Clearly perturbation with SO_2 prolongs the characteristic times. Furthermore, the perturbation effect increases with SO_2/H_2 ratio and decreases with T. The increase of characteristic times is due mainly to the depletion of O atoms by R_{31}, so the H-atom production rate by R_2 is reduced. This, in turn, reduces the branching rate of R_1.

The presence of large amount of HO_2 radicals in our experimental systems (low temperatures, T = 970–1150 K and SO_2-perturbed lean H_2/O_2/Ar mixture compositions), convinced us to include reactions between SO_2 and HO_2. Three possible reactions are R_{-47} ($HOSO + O_2 \leftarrow SO_2 + HO_2$), R_{-50} ($HSO_2 + O_2 \leftarrow SO_2 + HO_2$), and R_{56} ($SO_2 + HO_2 \rightarrow SO_3 + OH$). The first two reactions (R_{-47} and R_{-50}) have already included in the reaction mechanism of Rasmussen et al. [26] that was adopted in this work without any modification. R_{56} has been studied experimentally at low temperatures ($T < 300$ K) for atmospheric applications [35–38] and theoretically at high temperatures for combustion applications [39,40] (see the section Discussion). The inclusion of the reaction R_{56}, which has some sensitivity on the characteristic times (Fig. 1), is necessary to unravel the contributions by R_{31} and R_{56} to the disproportionate enhancement of the characteristic times with $[SO_2]_0$.

Using the Table 2 mechanism, computer simulations for experimental observables have been performed to simultaneously determine the rate coefficients of R_{31} ($SO_2 + O + M \rightarrow SO_3 + M$) and R_{56} ($SO_2 + HO_2 \rightarrow SO_3 + OH$). Determination of the rate coefficients was accomplished using a method similar to the solution mapping [41,42], i.e., for each experiment, only the k_{31} and k_{56} were systematically varied and the corresponding values of the function, $\Gamma(\boldsymbol{x}) = \Sigma_i[(\tau_{i,calculated}(\boldsymbol{x}) - \tau_{i,experimental})/\tau_{i,experimental}]^2$, where $i = \{\tau_{25}, \tau_{50}, \tau_{75}, \tau_{max}\}$ and $\boldsymbol{x} = \{\boldsymbol{k}_{31}, \boldsymbol{k}_{56}\}$, were calculated. Then an exhaustive search was made for the minimum value of $\Gamma(x)$ to find the optimized values of $x = \{k_{31}, k_{56}\}$. A simulated absorption profile is shown in Fig. 2. The resulting rate coefficients of R_{56} and R_{31} are plotted in Figs. 5 and 6, respectively. Experimental conditions, measured observables, and the rate coefficients determined for individual experiments are given in Table 3 in the Supporting Information.

DISCUSSION

No measurements had been made for the reactions between SO_2 and HO_2 at combustion temperatures. Three room temperature measurements have been made and calculations have been performed for combustion temperatures. Three product channels have been considered: R_{-47} ($HOSO + O_2 \leftarrow SO_2 + HO_2$), R_{-50} ($HSO_2 + O_2 \leftarrow SO_2 + HO_2$), and R_{56} ($SO_2 + HO_2 \rightarrow SO_3 + OH$). As for the first two reactions, included in the reaction mechanism of Rasmussen et al. [26] and also used

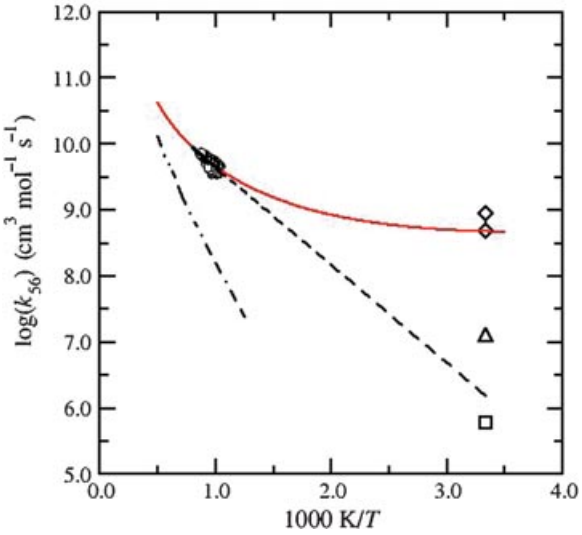

Figure 5 Rate coefficients of R_{56} ($SO_2 + HO_2 \rightarrow SO_3 + OH$). Symbols are as follows: circle, our data; diamond, Payne et al. [36]; square, Graham et al. [37]; triangle, Burrows et al. [38]. Lines are solid, a least-squares fit to our data, $k_{56} = 1.36 \times 10^{11} \exp(-3420\ \mathrm{K}/T)\ \mathrm{cm^3\ mol^{-1}\ s^{-1}}$ at $T = 970$–1150 K with estimated error of ±30%; dashed, extrapolation of our expression to room temperature; light solid, a three-parameter fit of our data with the lower limit value of the room temperature data of Payne et al., $k_{56} = 1.5 \times 10^{-3}\ T^4 \exp(1100\ \mathrm{K}/T)\ \mathrm{cm^3\ mol^{-1}\ s^{-1}}$ at $T =$ 300–2000 K; dot–dashed, calculated from $k_{-56} = 4.8 \times 10^4\ T^{2.46} \exp(-13720\ \mathrm{K}/T)\ \mathrm{cm^3\ mol^{-1}\ s^{-1}}$ of Hindiyarti et al. [39] with $K_{c,56}$. [Color figure can be viewed in the online issue, which is available at www.interscience.wiley.com.]

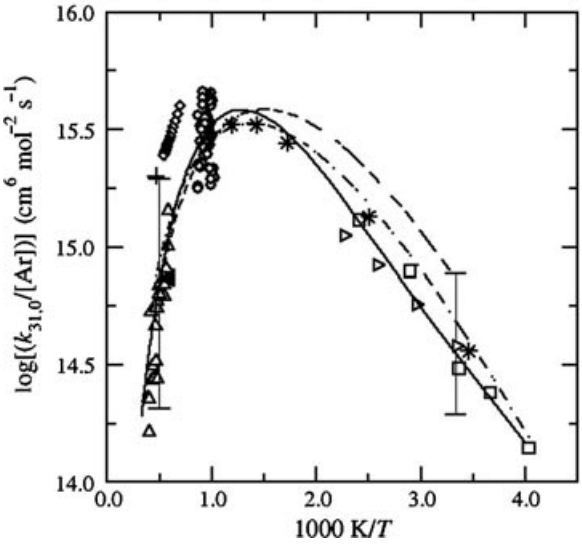

Figure 6 Low-pressure limits rate coefficient data of R_{31}. Symbols are as follows: plus, Nettleton and Stirling [45]; open square, Westenberg and deHaas [16]; open triangle up, Astholz et al. [18,19]; open triangle right, Atkinson and Pitts [17]; filled triangle left, Merryman and Levy [44]; open diamond, values from the rate coefficient expression of Smith et al. [20]; star, Naidoo et al. [22]; open circle, this study. Lines are (in $\mathrm{cm^6\ mol^{-2}\ s^{-1}}$) long dashed, Troe [21], $k_{31,0}/[\mathrm{Ar}] = 4.0 \times 10^{28}\ T^{-4.0} \exp(-2650\ \mathrm{K}/T)$, $T = 300$–2500 K; dot–dashed, Naidoo et al. [22], $k_{31,0}/[\mathrm{Ar}] = 2.4 \times 10^{27}\ T^{-3.6} \exp(-2610\ \mathrm{K}/T)$, $T = 220$–2500 K; solid, this study, $k_{31,0}/[\mathrm{Ar}] = 2.9 \times 10^{35}\ T^{-6.0} \exp(-4780\ \mathrm{K}/T) + 6.1 \times 10^{24}\ T^{-3.0} \exp(-1980\ \mathrm{K}/T)$, $T = 300$–2500 K. The average deviation of the high temperature experimental data of Astholz et al. ($T > 1700$ K) [18,19] from our fit is ca. ±30%.

in this study, there have been no experimental studies. For the third reaction channel, only the room temperature rate coefficients are available [35–38], which vary from $k_{56} \leq 6.0 \times 10^5$ to $k_{56} = 5.2 \times 10^8\ \mathrm{cm^3\ mol^{-1}\ s^{-1}}$. Of these, the two studies (Graham et al. [37] and Burrows et al. [38]) using direct in situ spectroscopic measurements of the reactants observed no measurable reaction with SO_2 and thus returned only upper limit values. The lower of these, Graham et al. [37], perforce obviates the other. Reaction with SO_2 was observed using the somewhat indirect photochemical $^{18}O_2$ competitive isotope-labeling technique method of Payne et al [36]; however, on the basis of a steady-state analysis of their kinetic scheme, they argue that the rate of R_{56} directly depends upon the ratio of isotopically labeled CO_2 produced in their reactor. The large discrepancy between these studies has not been thoroughly explored and remains a bit of a mystery. Indeed, all three room temperature determinations may have been affected by unforeseen problems with handling the reactants or by unforeseen subtleties and complications in the overall reaction systems used. A glimmer of this is perhaps the negative reaction rate observed by Graham et al. at their higher SO_2 concentration. To date, the generally accepted community value for R_{56} is that of Graham et al. recommended by the IUPAC Subcommittee on Gas Kinetic Data Evaluation for Atmospheric Chemistry [35].

Recently, there have been two theoretical investigations of R_{56} going to products relevant to combustion conditions. Hindiyarti et al. [39] performed ab initio energy and structure calculations coupled to transition state theory (TST) to obtain a rate coefficient expression for k_{-56} ($SO_2 + HO_2 \leftarrow SO_3 + OH$) given as $4.8 \times 10^4\ T^{2.46} \exp(-13720\ \mathrm{K}/T)\ \mathrm{cm^3\ mol^{-1}\ s^{-1}}$ in the temperature range of 800–2000 K. Wang and Hou [40] investigated the complicated reaction pathways leading from $SO_2 + HO_2$ to the various products and posited that the effectively barrier-free $HOSO + O_2$ (R_{-47}) channel is the dominant reaction at "normal" temperature. Their argument can be presented in a simple form as the competitive play between reaction dynamics and reaction energetics: R_{-50} ($HSO_2 + O_2 \leftarrow$

$SO_2 + HO_2$) is both kinetically and thermochemically disfavored (high barrier height and high endothermicity), R_{56} is kinetically disfavored but thermochemically favored (a moderate barrier but strong exothermicity), and R_{-47} is kinetically favored but thermochemically disfavored (no effective barrier but moderate endothermicity). Based upon this argument, only the rate coefficients for R_{-47} (and stabilization of the intermediate complex, important near room temperature) were calculated using TST and a master equation analysis. The results pass through the middle of the room temperature experimental data and are claimed to support the IUPAC evaluation. It should be noted that the difference between the calculated endothermicity of R_{-47} and the calculated barrier height for R_{56} is only 35 kJ mol^{-1} for their RCCSD(T)-cf calculation. Furthermore, while they do a good job of calculating the endothermicity of R_{-50} and R_{56} they may be low for R_{-47} (see their Table 1). As both R_{-47} and R_{56} are competitive channels that pass through the same intermediate complex, increasing the endothermicity of R_{-47} increases the relative flux through the R_{56} channel making it a significant reaction pathway. Even so, accepting Wang and Hou's basic argument we would still expect no net flux, and thus no significant effect upon the course of reaction, for the R_{-47} channel given the excess O_2 in our system and the barrier-free reverse reaction back to reactants for that channel. This was borne out in our simulations where we found that contribution to SO_2 oxidation by either R_{47} (R_{-47}) or R_{50} (R_{-50}) is insignificant under our experimental conditions (T = 970–1150 K). Rather, R_{56} plays an increasingly important role as the temperature is lowered and the SO_2 concentration is raised. For instance, using our highest SO_2 mixture, $SO_2/H_2/O_2/Ar$ = 3.0/0.5/10.0/86.5, at T = 1033 K and P = 1.45 atm, ca. 32% of SO_3 was formed by R_{56}, whereas ca. 66% of SO_3 was formed by R_{31} at times between 0.5 and 2.0 ms; while for our lowest SO_2 mixture $SO_2/H_2/O_2/Ar$ = 1.0/0.5/10.0/88.5 at T = 996 K and P = 1.31 atm, ca. 16% of SO_3 was formed by R_{56}, whereas ca. 82% of SO_3 was formed by R_{31} at the same time interval. The optimized k_{56} values are plotted in Fig. 5 together with those of Hindiyarti et al. calculated from $K_{C,56}$, and the various room temperature measurements. Our data are well fitted as

$$k_{56} = 1.36 \times 10^{11} \exp(-3420\,\mathrm{K}/T)\ \mathrm{cm^3\ mol^{-1}\ s^{-1}}$$

at T = 970–1150 K with estimated error limits of ± 30% and is shown as the dark solid line, which is extrapolated to room temperature (dashed line). It is interesting to note that the room temperature value of our expression is not far above the upper limit value of Graham et al. [37], the value recommended by the IUPAC Subcommittee on Gas Kinetic Data Evaluation for Atmospheric Chemistry [35]. As an enlightening exercise, we can find an equally good fit to our data by employing a gentle upwardly curving expression (of the basic form predicted by Wang and Hou [40]) that passes through the data of Payne et al [36]. This is shown as the light solid line in Fig. 5. Indeed, due to experimental scatter and the relatively narrow temperature range our data appear as essentially a single point on a graph like Fig. 5. Thus we can always find a good curve fit that passes through both our data and nearly any given room temperature value. Our data cannot help elucidate the rate of this reaction at lower temperatures. As we have noted earlier, this channel becomes more important with decreasing temperature and so can play an important role in combustion exhaust.

Our $k_{31,\mathrm{eff}}$ values show, first, a very slight negative temperature dependence at T = 970–1150 K and ρ_{ave} = 16.2 μmol cm^{-3} and second, about 15–30% higher than those from $k_{31,0}$ expression of Naidoo et al. [22] at the same conditions. This is the indirect indication that we obtained the low-pressure limit rate coefficients ($k_{31,0}$). Thus, at each experimental condition, $k_{31,0}$/[M] was obtained by scaling $k_{31,0}$ with the corresponding collision-efficiency-corrected density, $[M] = \rho \times [1 + x_{O_2}(\varepsilon_{O_2} - 1) + x_{SO_2}(\varepsilon_{SO_2} - 1)]$. Here the collision efficiencies are $\varepsilon_{O2} = 1.3$, $\varepsilon_{SO_2} = 9.0$ and $\varepsilon_{\mathrm{other\ species}} = 1.0$, including ε_{Ar}. The $k_{31,0}$/[Ar] values obtained in this manner are listed in Table 3 in the Supporting Information and plotted in Fig. 6.

All possible uncertainties in our $k_{31,0}$/[Ar] values are estimated as follows: The presence of H atoms from sources other than the initiation reaction, R_{-11} ($HO_2 + H \leftarrow H_2 + O_2$), and the uncertainty in $[SO_2]_0$ are considered first. The effect of H-atom impurity was explored by injecting $[H]_0$ = 0.1 ppb into the system—this $[H]_0$ is about five times larger than the kinetically produced $[H]_0$ in our experimental conditions. The $k_{31,0}$ values were increased by less than 20% and 3% with 1.0% $SO_2/H_2/O_2/Ar$ mixture and 3.0% $SO_2/H_2/O_2/Ar$ mixture, respectively. The effect of the 0.5% uncertainty in the nominal $[SO_2]_0$ mole fractions was negligible. Here we placed a factor of 1.2 uncertainties in $k_{31,0}$ owing to the possible presence of impurity as H atoms.

The influence of the uncertainties from other reaction rate coefficients on the determination of $k_{31,0}$/[Ar] is examined next. As seen in the sensitivity figure, R_9 ($H + O_2 + M \rightarrow HO_2 + M$) exhibits the largest sensitivity. For the rate coefficients of R_9 we used $k_{9,0}/[Ar] = 5.55 \times 10^{18}\ T^{-1.15}$ $cm^6\ mol^{-2}\ s^{-1}$ of Hwang et al. [24] with uncertainty limits of 30%. The uncertainties in $k_{31,0}$/[Ar] due to the coupling between R_{31} and R_9 were estimated by varying the rate coefficients of R_9 of

Hwang et al. by the given uncertainty limits and then observing the propagated effects on $k_{31,0}$/[Ar]. With 30% reduction of $k_{9,0}$/[Ar], the resulting changes in $k_{31,0}$/[Ar] are 90%, 50%, and 40% for 1.0%, 2.0%, and 3.0% $SO_2/H_2/O_2$/Ar mixtures, respectively. But, for 1.0% SO_2 mixtures, the changes in reaction profiles were so great that reasonable matches to the characteristic times with any combination of $k_{31,0}$/[Ar] and k_{56} could not be achieved satisfactorily. We put a factor of 1.6 uncertainties on $k_{31,0}$/[Ar] due to the coupling of R_{31} with R_9. In the presence of SO_2, H atoms formed in the H_2/O_2 system are also consumed by R_{29} ($SO_2 + H (+M) \rightarrow HOSO (+M)$). The rate coefficient expressions of R_{29} ($k_{29,0}$/[M] and $k_{29,\infty}$) are those of Blitz et al. [43]. We used our conservative error limit estimate of ±30% for k_{29}. The ±30% variation of k_{29} resulted in less than 20% change of $k_{31,0}$/[Ar]. So we set a factor of 1.2 uncertainties on $k_{31,0}$/[Ar]. The effect of R_{14} ($HO_2 + OH \rightarrow H_2O + O_2$) on $k_{31,0}$/[Ar] via R_{56} ($SO_2 + HO_2 \rightarrow SO_3 + OH$) was ca. 6% when k_{14} values were reduced by ca. 35%. Here we set a factor of 1.1 uncertainties on $k_{31,0}$/[Ar] (see details below).

The differences between the experimental and computed characteristic times for individual runs are on average less than 2% for τ_{50} and τ_{75} and 4% for τ_{25} and τ_{max}. Taking into account all of the uncertainties discussed above plus additional uncertainties for P_0, shock speed, signal-to-noise ratio, etc., we estimated maximum uncertainty limits, $U = \sqrt{\Sigma U_i^2} \cong 3.0$ for individual runs.

A good fit to the data of this study and the previous experiments [16–19,22,44,45] is found using a combination of two non-Arrhenius-type expressions given as

$$k_{31,0}/[\mathrm{Ar}] = 2.9 \times 10^{35} T^{-6.0} \exp(-4780\,\mathrm{K}/T) + 6.1 \times 10^{24} T^{-3.0} \exp(-1980\,\mathrm{K}/T)\,\mathrm{cm}^6 \times \mathrm{mol}^{-2}\,\mathrm{s}^{-1}$$

at $T = 300$–2500 K. As seen in Fig. 6, our data show the largest scatter. The rate coefficient expression shown above represents all the data within 26% error limits. Although we were unable to perform this study using N_2 as a collider gas, those modeling this reaction in Air might want to use the commonly referenced collider efficiency ratio of 0.77 (Ar/N_2) recommended by Atkinson et al. [35].

The rate coefficients from our expression are compared with those of previous studies. At $T = 1050$ K, the rate coefficient (in unit of $cm^6\ mol^{-2}\ s^{-1}$) from the above equation (3.1×10^{15}) is about a factor of 7 and 3 smaller than the extrapolated value of Astholz et al. (2.2×10^{16}) [18,19] and Smith et al. (9.0×10^{15}) [20], respectively. But it is about 15% larger than the fit of Troe (2.7×10^{15}) [21] and RRKM fit of Naidoo et al. (2.7×10^{15}) [22]. There is a competition for SO_2 between O and HO_2. If HO_2 loss due to R_{14} ($HO_2 + OH \rightarrow H_2O + O_2$) were increased, then there would be more SO_2 available and the overall reaction would be delayed even more. This would then require a decrease in $k_{31,0}$/[Ar] to account for the observed characteristic times, particularly at both low $[SO_2]_0$ and low-temperature conditions. The reverse argument is also true, and there is a range of k_{14} values to choose among (see below). Using the lowest reported k_{14} expression, Kappel et al. [46], instead of Srinivasan et al. [25] used in this study, only increases the $k_{31,0}$/[Ar] values by 6% at our most sensitive conditions.

The situation for R_{14} is certainly confusing at this time as can be seen in the rather busy nature of Fig. 7. The reaction has been studied quite extensively, both directly and indirectly, both experimentally and computationally, by numerous techniques covering the temperature range relevant from atmospheric chemistry to flames. There is general agreement that the rate coefficient values of Keyser [47] at low temperatures and Goodings and Hayhurst [48] at high temperatures are firmly rooted; for the midtemperature range

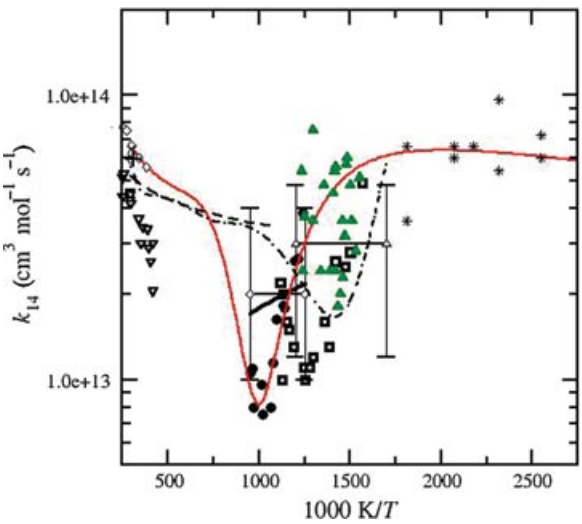

Figure 7 Rate coefficients of R_{14} ($HO_2 + OH \rightarrow H_2O + O_2$). Symbols are as follows: plus, Cox et al. [56]; open triangle down, Sridharan et al. [57]; star, Goodings and Hayhurst [48]; open diamond, Keyser [47]; open square, Hippler et al. [50]; filled circle, Kappel et al. at $P = 4$ bar [46]; filled triangle up, Srinivasan et al. [25]. Lines are (in $cm^3\ mol^{-1}\ s^{-1}$): solid connecting two open diamonds, Hippler and Troe [49]; dashed, Gonzalez et al. [54]; solid, Kappel et al. [46]; solid connecting two open triangles up, Srinivasan et al. [25]; dot–dashed, Sivaramakrishnan et al. [52]; light solid, Rasmussen et al. [51]. [Color figure can be viewed in the online issue, which is available at www.interscience.wiley.com.]

of interest in this study, the values are still in flux. Troe and coworkers [46,49,50] have published a series of increasingly refined shock tube measurements of R_{14} using various optical diagnostics to measure OH, HO_2, and H_2O_2 temporal profiles. As can be seen in Fig. 7, their earlier data (930–1680 K) [50] had a deep and narrow "V" temperature dependence centered around 1250 K (open square). Their later data [46] had a similar but less pronounced feature centered around 1000 K (filled circle). Nevertheless, they reported rate coefficient expressions that were either a straight line, $k_{14} = (2 \pm 1) \times 10^{13}$ cm^3 mol^{-1} s^{-1} at $T = 1000$–1250 K [49] (solid line connecting two open diamonds), or an imperceptibly curved line, $k_{14} = 1.0 \times 10^{13} + 5.8 \times 10^{13} \exp(-2000\ \mathrm{K}/T)$ cm^3 mol^{-1} s^{-1} at $T = 950$–1250 K [46] (dark solid line). More recently, Srinivasan et al. [25] performed a direct determination of k_{14} values via a joint optimization of the reactions $OH + NO_2 \rightarrow HO_2 + NO$ and $HO_2 + OH \rightarrow H_2O + O_2$ (R_{14}) reactions behind reflected shocks using an OH diagnostic. Their recommended rate coefficient expression is $k_{14} = (3.0 \pm 1.8) \times 10^{13}$ cm^3 mol^{-1} s^{-1} at $T = 1200$–1700 K (solid line connecting two open triangles up)— this k_{14} expression was used throughout this study. This expression is 25% lower than the best fit to their data, but they concluded that it is the best available experimental value for combustion-modeling applications based upon their consideration of other high-temperature data. Rasmussen et al. [51] performed a critical review of all the available data for this reaction as part of the analysis of their high-pressure laminar flow measurements of the $CO/H_2O/O_2/NO_x$ reaction system. In their temperature range, 600–900 K, there are no experimental measurements of R_{14}. They proposed an expression that is the sum of three three-parameter rate coefficient expressions that does an excellent job of fitting the high-temperature data of Goodings and Hayhurst and Kappel et al., including the sharp dip, as well as the low-temperature data of Keyser. It also passes through the data of Srinivasan et al. (filled triangle up). Their expression is a factor of 3 lower than ours on average in the range of mutual overlap. Sivaramakrishnan et al. [52] derived an expression for k_{14} indirectly as a result of their high pressure single pulse shock tube study of the oxidation of diluted CO mixtures doped with small quantities of H_2. Their expression is given as the sum of five three-parameter rate coefficient expressions over the temperature range 298–1600 K that produces a narrow dip at $T = 1400$ K (dot–dashed line). They argue that this expression is needed to match their CO and CO_2 concentration data at their highest temperatures, 1400–1500 K, and their highest pressures, 256 and 450 atm. The dip in their expression at 1400 K is shifted upward in temperature with respect to Hippler et al. (1250 K) and Kappel et al. (1000 K); it is also neither as deep nor as sharp. The Sivaramakrishnan et al. and our k_{14} expressions agree within 10% over the temperature range of mutual overlap. Their expression decreases with temperature in this range, and they are mostly above us with the expressions crossing ca. 1075 K (the upper third of our temperature range). The most recent theoretical study of R_{14} has been performed by Gonzalez et al. [53,54] (see references therein for a thorough review of previous theoretical work), where they determined ab initio geometries at the HF and MP2 levels and energies at the MP4 level. They are careful to detail the problems with calculating the surfaces at this level of theory. For the singlet reaction surface, they determined that this pathway would be unimportant near room temperature, their area of focus, due to the 63.6 kJ mol^{-1} barrier heights. For the triplet reaction surface, they do predict that reaction can occur at room temperature. However, they cautioned that their calculations were not sufficiently adequate to quantitatively determine the coupling between the nonplanar surfaces at the MP2 level. Given that caveat, they moved forward to predict a rate coefficient expression using vibrational/rotational adiabatic theory. Their calculated temperature dependence of k_{14} values was then combined with the room temperature experimental data to produce the best estimate of the k_{14} expression given as $k_{14} = 4.3 \times 10^{13} (T/300)^{-0.21} \exp(57\ \mathrm{K}/T)$ cm^3 mol^{-1} s^{-1} at $T = 298$–1100 K (dashed line).

The direct experimental evidence has produced three effectively straight line rate coefficient expressions, each within the error bars of the others, all lying within the range $(2$–$3) \times 10^{13}$ cm^3 mol^{-1} s^{-1} and overlapping around 1250 K. It cannot be overemphasized that none of them shows any evidence of the narrow "V" behavior. The indirect experimental evidence has produced a very complex expression but one that is within 10% of the Srinivasan et al. expression used in this study around 1000 K and well within the error bars of all three direct studies. The available theoretical evidence, while carefully qualified by its authors, gives a very mildly curved rate coefficient expression that passes through the error bars of the direct experiments. Combining the published data given in the three studies with the low-temperature data of Keyser and the high-temperature data of Goodings and Hayhurst would strongly suggest the same sort of broad and shallow bowl-shaped appearance that is the signature of the HO_2 self-reaction. Clearly, the advances made by the theoretical community during the intervening decades since the most recent computational study would help to elucidate the nature of this important reaction and guide future experiments.

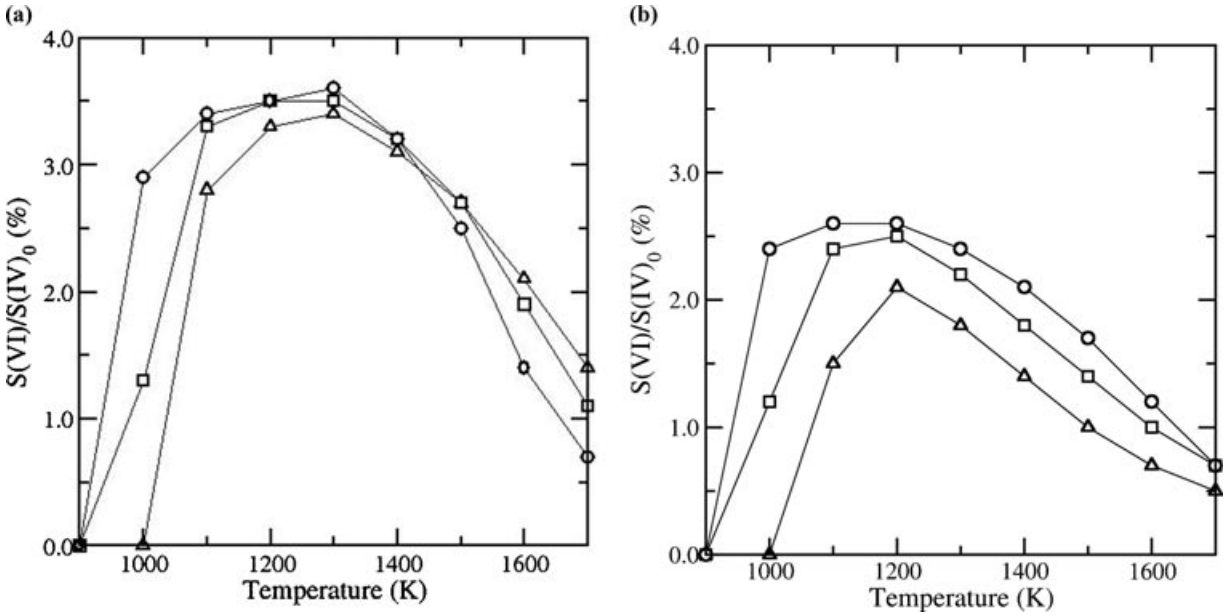

Figure 8 (a) Conversion yield of S(IV) to S(VI), calculated at a constant density condition ($\rho = 16.0$ μmol cm^{-3}) using the Table 2 mechanism as functions of temperature and reaction (residence) time. Symbols are for reaction time: triangle, 1 ms; square, 2 ms; circle, 5 ms. (b) Conversion yield calculated at a constant pressure condition ($P = 1$ atm). Symbols are as in panel a.

Among our mixtures, 1.0% SO_2 gave the highest conversion yield of S(IV) to S(VI), i.e., SO_2 to SO_3 (the contribution to S(VI) from $HOSO_2$ and H_2SO_4 being negligible at our experimental conditions). Thus we computed the maximum conversion, $[SO_3]_{max}/[SO_2]_0$, in the $SO_2/H_2/O_2/Ar = 1.0/0.5/10.0/88.5$ mixture using the Table 2 mechanism as functions of temperature and reaction time (residence time) at a constant density ($\rho = 16.0$ μmol cm^{-3}) and a constant pressure ($P =$ 1.0 atm) flow conditions. As seen in Figs. 8a and 8b, for either flow condition, maximum conversion occurs at temperatures around 1200 K and slightly increases with reaction time. The maximum conversion yield is ca. 3.5% and 2.5% for the constant density and constant pressure flow condition, respectively. Flux analyses show that SO_3 is mainly produced by R_{31} ($SO_2 + O + M \rightarrow SO_3 + M$). At low temperatures, there is some contribution from R_{56} ($SO_2 + HO_2 \rightarrow SO_3 + OH$). The major consumption channels are R_{34} ($SO_3 + H \rightarrow SO_2 + OH$), R_{35} ($SO_3 + O \rightarrow SO_2 + O_2$) and R_{-52} ($HOSO_2 + O_2 \leftarrow SO_3 + HO_2$). It is noteworthy that the maximum conversion occurs at temperatures above that of the maximum $k_{31,0}$ values. Undoubtedly, this is because that the conversion yield is dependent upon not only the rate coefficient values of $k_{31,0}$ and k_{56} but also the availability (concentrations) of H, O, and HO_2 in the system.

The unusual behavior in the rate coefficients of the spin-forbidden title reaction, R_{31} ($SO_2(X^1A_1) + O(^3P) + M \rightarrow SO_3(X^1A_1') + M$) has been rationalized by Astholz et al. [19] in terms of the potential barrier arising from triplet–singlet crossing of the SO_3 complex formed ($SO_3(^3A') \rightarrow SO_3(^1A')$) and decrease of the collision efficiency (β_c) with temperature in stabilizing the collision complex, i.e., the rate coefficients are controlled by the competition between the barrier crossing and the stabilization of the complex. Astholz et al. used $V_0 = 13.8 \pm 4$ kJ mol^{-1} and a factor of 4 decrease of β_c from 300 K ($\beta_c = 0.4$) to 2000 K ($\beta_c = 0.1$), whereas Naidoo et al. [22] used 15.9 kJ mol^{-1} in their calculations. However, for understanding of this reaction in more detail, high-level quantum calculations are beneficial to elucidate the nature of the triplet SO_3 potential curve—it may be repulsive around the crossing—and the coupling between triplet–singlet states. Recognizing the triplet–singlet crossing actually occurs along the seam at the lowest crossing point, it is highly desirable to calculate the potential energy surface (PES) around the crossing point. If the seam crossing probability is energy dependent, a new temperature effect could be introduced.

We now consider the possibility of SO_3 formation by a molecular reaction channel involving the relatively abundant amounts of SO_2 and O_2 available in the hot oxidizing environment of the high-pressure section of an aircraft engine. The most efficient version of the reaction would be the direct oxidation of SO_2 to SO_3 in the form of R_{58} ($SO_2 + SO_2 + O_2 \rightarrow SO_3 + SO_3$).

Such a reaction may be viewed as proceeding, similar to $S_2O_6^-$ reactions [55], via $SO_2 + O_2 \rightarrow SO_4 + SO_2 \rightarrow O_3SOSO_2 \rightarrow SO_3 + SO_3$ or $SO_2 + SO_2 + O_2 \rightarrow O_2SOOSO_2 \rightarrow SO_3 + SO_3$. Compared to $S_2O_6^-$ fragmentation reactions, either reaction shown above does not have an available donor electron for easy fragmentation to SO_3. Also a large number of rearrangements for intermediate formation would be required, so that high reaction rate coefficient values are not expected. Nevertheless, we can assign a maximum value to the rate coefficient of R_{58} at our test conditions based upon the observed flatness of the absorption profile preceding the exponential rise due to chain reaction. The proposed molecular reaction would start at time zero and be evidenced by a steady decrease in the initial absorption, entirely due to SO_2, as expected for a mixture containing both the reactants. The k_{58} value was chosen such that visible change in the initial absorption signal, greater than our signal-to-noise ratio was noticed. For our conditions, $k_{58} = 3.0 \times 10^{12}$ cm^6 mol^{-2} s^{-1} was chosen (the reverse rate coefficient was calculated via $K_{c,58}$). First, we chose the highest SO_2 mixture run at the lowest temperature and second, because the influence to the conversion yield from S(IV) to S(VI) by R_{58} would increase with the increase of $[SO_2]_0$ and decrease with T, we selected a test condition of $T = 1050$ K and $\rho = 16.0$ μmol cm^{-3} in 3.0% SO_2-containing mixture. As seen in Fig. 9, the characteristic times (τ_{25}, τ_{50}, τ_{75}, and τ_{max}) were shortened by ca. 13% and the maximum normalized growth constant of the absorption signal ($[dA(t)/dt/A_{max}]_{max}$)—shape of the absorption signal—was increased by ca. 20%. With the increase of only the $k_{31,0}$ value by 26% (still within our stated upper error limit), satisfactory agreement was achieved in both the characteristic times and the maximum normalized growth constant. At high temperatures for 3%, 2%, and 1% SO_2-containing mixtures (1150, 1150, and 1040 K, respectively), however, the simulated absorption profiles with inclusion of R_{58} showed no alteration of the reaction characteristics. The changes in the low temperature $\{\tau_i\}$ values are due to reduction of reaction flux through R_{31} ($SO_2 + O + M \rightarrow SO_3 + M$) by depletion of available $[SO_2]$ by R_{58} ($SO_2 + SO_2 + O_2 \rightarrow SO_3 + SO_3$).

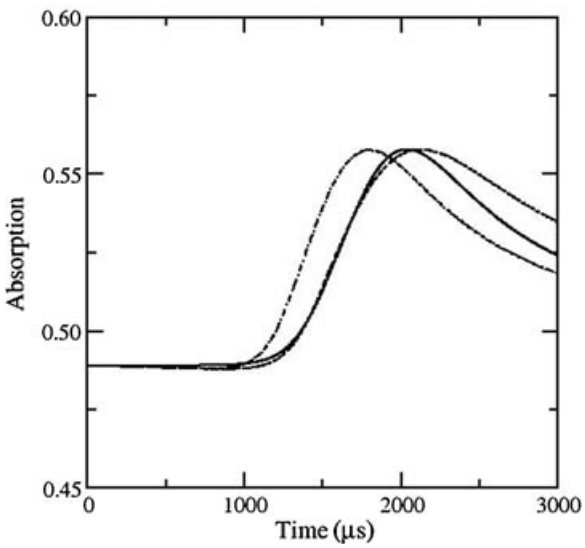

Figure 9 Simulated absorption profiles using the Table 2 mechanism with and without R_{58} ($SO_2 + SO_2 + O_2 \rightarrow SO_3 + SO_3$) for the condition of $SO_2/H_2/O_2/Ar$ = 3.0/0.5/10.0/86.5, $T = 1050$ K and $\rho = 16.0$ μmol cm^{-3}. Lines are solid, without R_{58}; dot–dashed, with R_{58} and $k_{58} = 3.0 \times 10^{12}$ cm^6 mol^{-1} s^{-1}; dashed, with R_{58} ($k_{58} = 3.0 \times 10^{12}$ cm^6 mol^{-1} s^{-1}) and $k_{31,0}$ ($SO_2 + O + M \rightarrow SO_3 + M$) × 1.26.

With the inclusion of R_{58}, as expected, we observed some increase of the conversion yields at all temperatures for the 3% and 2% SO_2-containing mixtures. For example, with the rate coefficient and test conditions given above the conversion yield was increased from 1.7% to 2.5% at 5 ms where the maximum conversion occurs. We also observed the increase of the conversion yield at all temperatures for the 3% and 2% SO_2-containing mixtures.

It is apparent that R_{58} affects the characteristic times and conversion yields for high $[SO_2]_0$-containing mixtures. But the extent of the effect is not large: As shown above, agreement in the characteristic times with and without R_{58} could be achieved by increasing $k_{31,0}$ value within its error limit. And the absolute values of the conversion yield with R_{58} are still small. Lack of experimental or theoretical evidence for R_{58} and the reasons given above permitted us to exclude R_{58} in the Table 2 mechanism.

CONCLUSIONS

Thermochemical and structural data for HOSO, HSO_2, and $HOSO_2$ were critically reviewed, and the thermodynamic data for these species were estimated and NASA-type polynomial coefficients were established (Table 1 in the Supporting Information).

The title reaction was studied in the perturbed systems where the well-studied $H_2/O_2/Ar$ system was perturbed with small amounts of SO_2. A comprehensive reaction mechanism for $SO_2/H_2/O_2/Ar$ system was assembled (Table 2 in the Supporting Information). Optimum $SO_2/H_2/O_2/Ar$ mixture compositions and experimental conditions were obtained via a series of sensitivity analyses. Shock tube experiments were performed using an OH laser absorption spectroscopic technique. The measured absorption coefficients of

SO_2 at $\lambda_0 = 310.032$ nm (air) and $T = 300$–1150 K are

$$\varepsilon_e(SO_2) = 1.3 \times 10^5 \exp(-180\,\mathrm{K}/T)\,\mathrm{cm}^2\,\mathrm{mol}^{-1}$$

The experimental results were analyzed via computer simulations, in that the rate coefficients of R_{31} ($SO_2 + O + M \rightarrow SO_3 + M$) and R_{56} ($SO_2 + HO_2 \rightarrow SO_3 + OH$) were simultaneously optimized against the experimental reaction characteristics (characteristic times). The rate coefficient expressions are

$$k_{56} = 1.36 \times 10^{11} \exp(-3420\,\mathrm{K}/T)\,\mathrm{cm}^3\,\mathrm{mol}^{-1}\,\mathrm{s}^{-1}$$

at $T = 970$–1150 K with estimated error limits of ± 30%, and

$$k_{31,0}/[\mathrm{Ar}] = 2.9 \times 10^{35}\, T^{-6.0} \exp(-4780\,\mathrm{K}/T) + 6.1 \times 10^{24}\, T^{-3.0} \exp(-1980\,\mathrm{K}/T) \times \mathrm{cm}^6\,\mathrm{mol}^{-2}\,\mathrm{s}^{-1}$$

at $T = 300$–2500 K and $\rho_{ave} = 16.2$ μmol cm^{-3} with error limits of 26%.

The calculated maximum S(IV) to S(VI) conversion yield, ca. 3.5% and 2.5% for the constant density and constant pressure flow condition, respectively, occurred at rather higher temperatures (∼1200 K) than lower where the maximum $k_{31,0}$ value is located (∼800 K). We found that the conversion yield is controlled by SO_3 production flux mainly through R_{31} ($SO_2 + O + M \rightarrow SO_3 + M$) and, to the lesser extent, through R_{56} ($SO_2 + HO_2 \rightarrow SO_3 + OH$) and consumption flux through the reactions with H (R_{34}, $SO_3 + H \rightarrow SO_2 + OH$), O ($R_{35}$, $SO_3 + O \rightarrow SO_2 + O_2$) and HO_2 (R_{-52}, $HOSO_2 + O_2 \leftarrow SO_3 + HO_2$) as well.

All experiments and computations in this study were performed at the NASA Glenn Research Center in Brook Park, Ohio.

BIBLIOGRAPHY

1. Meerkotter, R.; Schumann, U.; Doelling, D. R.; Minnis, P.; Nakajima, T.; Tsushima, Y. Ann Geophys 1999, 17, 1080–1094.
2. Duda, D. P.; Minnis, P.; Nguyen, L. J Geophys Res 2001, 106, 4927–4937.
3. Travis, D. J.; Carleton, A. M.; Lauritsen, R. G. Nature 2002, 418, 601.
4. Arnold, F.; Scheid, J.; Stilp, T.; Schlager, H.; Reinhardt, M. E. Geophys Res Lett 1992, 12, 2421–2424.
5. Busen, R.; Schumann, U. Geophys Res Lett 1995, 22, 1357–1360.
6. Fahey, D. W.; Keim, E. R.; Woodbridge, E. L.; Gao, R. S.; Boering, K. A.; Daube, B. C.; Wofsy, S. C.; Lohmann, R. P.; Hintsa, E. J.; Dessler, A. E.; Webster, C. R.; May, R. D.; Brock, C. A.; Wilson, J. C.; Miake-Lye, R. C.; Brown, R. C.; Rodriguez, J. M.; Loewenstein, M.; Proffitt, M. H.; Stimpfle, R. M.; Bowen, S. W.; Chan, K. R. Geophys Res 1995, 100, 3065–3074.
7. Hoffmann, D. J.; Rosen, J. M. Geophys Res Lett 1978, 5, 511–514.
8. Kaercher, B.; Peter, T.; Ottmann, R. Geophys Res Lett 1995, 22, 1501–1504.
9. Zhao, J.; Turco, R. P. J Aerosol Sci 1995, 26, 779–795.
10. Curtius, J.; Sierau, B.; Arnold, F.; Baumann, R.; Busen, R., Schulte, P.; Schumann, U. Geophys Res Lett 1998, 25, 923–926.
11. Schumann, U.; Arnold, F.; Busen, R.; Curtius, J.; Kaercher, B.; Kiendler, A.; Petzold, A.; Schlager, H.; Schroeder, F.; Wohlfrom, K. -H. J Geophys Res 2002, 107, AAC 2-1–AAC 2-27.
12. Curtius, J.; Arnold, F.; Schulte, P. Geophys Res Lett 2002, 29, 17-1–17-4.
13. Fahey, D. W.; Keim, E. R.; Boering, K. A.; Brock, C. A.; Wilson, J. C.; Jonsson, H. H.; Anthony, S.; Hanisco, T. F.; Wennberg, P. O.; Miake-Lye, R. C.; Salawitch, R. J.; Louisnard, N.; Woodbridge, E. L.; Gao, R. S.; Donnelly, S. G.; Wamsley, R. C.; Del Negro, L. A.; Solomon, S.; Daube, B. C.; Wofsy, S. C.; Webster, C. R.; May, R. D.; Kelly, K. K.; Loewenstein, M.; Podolske, J. R.; Chan, K. R. Science 1995, 270, 70–74.
14. Schumann, U.; Stroem, J.; Busen, R.; Baumann, R.; Gierens, K.; Krautstrunk, M.; Schroeder, F.; Stingl, J. J Geophys Res 1996, 101, 6853–6869.
15. Schroeder, F.; Brock, C. A.; Baumann, R.; Petzold, A.; Busen, R.; Schulte, P.; Fiebig, M. J Geophys Res 2000, 105, 19941–19954.
16. Westenberg, A. A.; deHass, N. J Chem Phys 1975, 63, 5411–5415.
17. Atkinson, R.; Pitts, J. N., Jr. Int J Chem Kinet 1978, 10, 1081–1090.
18. Astholz, D. C.; Glaenzer, K.; Troe, J. Proceedings of the 11th International Shock Tube Symposium on Shock Tubes and Waves; University of Washington Press: Seattle, 1977; pp. 232–237.
19. Astholz, D. C.; Glaenzer, K.; Troe, J. J Chem Phys 1979, 70, 2409–2413.
20. Smith, O. I.; Tseregounis, S.; Wang, S. Int J Chem Kinet 1982, 14, 679–697.
21. Troe, J. Ann Rev Phys Chem 1978, 29, 223–250.
22. Naidoo, J.; Goumri, A.; Marshall, P. Proc Combust Inst 2005, 30, 1219–1225.
23. Hwang, S. M.; Cooke, J. A.; De Witt, K. J.; Rabinowitz, M. J. Poster No. 1F1-22. In 30th International Symposium on Combustion, University of Illinois at Chicago, Chicago, July 25–30, 2004.
24. Hwang, S. M.; Ryu, S. -O.; De Witt, K. J.; Rabinowitz, M. J. Chem Phys Lett 2005, 408, 107–111.

25. Srinivasan, N. K.; Su, M. -C.; Sutherland, J. W.; Michael, J. V.; Ruscic, B. J Phys Chem A 2006, 110, 6602–6607.
26. Rasmussen, C. L.; Glarborg, P.; Marshall, P. Proc Combust Inst 2007, 31, 339–347, and references therein.
27. Lovejoy, E. R.; Hanson, D. R.; Huey, L. G. J Phys Chem 1996, 100, 19911–19916.
28. Hwang, S. M.; Ryu, S.-O.; De Witt, K. J.; Rabinowitz, M. J. J Phys Chem A 1999, 103, 5949–5958.
29. McBride, B. J.; Zehe, M. J.; Gordon, S. NASA/TP 2002-211556; NASA: Washington, DC, 2002.
30. Burcat, A.; Ruscic, B. Third Millennium Thermodynamic Database of New NASA Polynomials with Active Thermochemical Tables Updates; Report ANL 05/20, TAE 960. Available at http://garfield.chem.elte.hu/Burcat/burcat.html, accessed Jan. 28, 2009.
31. Ryu, S. -O.; Hwang, S. M.; Rabinowitz, M. J. J Phys Chem 1995, 99, 13984–13991.
32. Gardiner, W. C., Jr.; Walker, B. F.; Wakefield, C. B. In Shock Waves in Chemistry; Lifshitz, A. (Ed.); Marcel Dekker: New York, 1981; Chap. 7.
33. Hwang, S. M.; Kojima, J. N.; Viet, Q.-V.; Rabinowitz, M. J. J Quant Spectrosc Radiat Transfer 2008, 109, 2715–2714.
34. Vandaele, A. C.; Simon, P. C.; Guilmot, J. M.; Carleer, M.; Colin, R. J Geophys Res 1994, 99, 25599–25605.
35. Atkinson, R.; Baulch, D. L.; Cox, R. A.; Crowley, J. N.; Hampson, R. F., Jr.; Hynes, R. G.; Jenkin, M. E.; Rossi, M. J.; Troe, J. Atmos. Chem. Phys. 2004, 4, 1461–1738.
36. Payne, W. A.; Stief, L. J.; Davis, D. D. J Am Chem Soc 1973, 14, 7614–7619.
37. Graham, R. A.; Winer, A. M.; Atkinson, R.; Pitts, J. N., Jr. J Phys Chem 1979, 83, 1563–1567.
38. Burrows, J. P.; Cliff, D. I.; Harris, G. W.; Thrush, B. A.; Wilkinson, J. P. T. Proc R Soc Lond A 1979, 368, 463–481.
39. Hindiyarti, L.; Glarborg, P.; Marshall, P. J Phys Chem A 2007, 111, 3984–3991.
40. Wang, B.; Hou, H. Chem Phys Lett 2005, 410, 235–241.
41. Hwang, S. M. PhD thesis, The University of Texas at Austin, 1988.
42. Frenklach, M.; Wang, H.; Rabinowitz, M. J. Prog Energy Combust Sci 1992, 18, 47–73.
43. Blitz, M. A.; Hughes, K. J.; Pilling, M. J.; Robertson, S. H. J Phys Chem A 2006, 110, 2996–3009.
44. Merryman, E. L.; Levy, A. Proc Combust Inst 1978, 17, 727–736.
45. Nettleton, M. A.; Stirling, R. Proc Combust Inst 1969, 12, 635–641.
46. Kappel, Ch.; Luther, K; Troe, J. Phys Chem Chem Phys 2002, 4, 4392–4398.
47. Keyser, L. J Phys Chem 1988, 92, 1193–1200.
48. Goodings, J. M.; Hayhurst, A. N. J Chem Soc, Faraday Trans 2 1988, 84, 745–762.
49. Hippler, H.; Troe, J. Chem Phys Lett 1992, 192, 333–337.
50. Hippler, H.; Neunaber, H.; Troe, J. J Chem Phys 1995, 103, 3510–3516.
51. Rasmussen, C. L.; Hansen, J.; Marshall, P.; Glarborg, P. Int J Chem Kinet 2008, 40, 454–480.
52. Sivaramakrishnan, R.; Comandini, A.; Tranter, R. S.; Brezinsky, K.; Davis, S. G.; Wang, H. Proc Combust Inst 2007, 31, 429–437.
53. Gonzalez, C.; Theisen, J.; Zhu, L.; Schlegel, H. B.; Hase, W. L.; Kaiser, E. W. J Phys Chem 1991, 95, 6784–6792.
54. Gonzalez, C.; Theisen, J.; Schlegel, H. B.; Hase, W. L.; Kaiser, E. W. J Phys Chem 1992, 96, 1767–1774.
55. McKee, M. J Phys Chem 1996, 100, 3473–3481.
56. Cox, R. A.; Burrows, J. P.; Wallington, T. J. Chem Phys Lett 1981, 84, 217–221.
57. Sridharan, U. C.; Qui, L. X.; Kaufman, F. J Phys Chem 1984, 88, 1281–1282.